Optical design of the Wide Angle Camera for the Rosetta mission

Giampiero Naletto, Vania Da Deppo, Maria Guglielmina Pelizzo, Roberto Ragazzoni, and Enrico Marchetti

The final optical design of the Wide Angle Camera for the Rosetta mission to the P/Wirtanen comet is described. This camera is an $F/5.6$ telescope with a rather large $12° \times 12°$ field of view. To satisfy the scientific requirements for spatial resolution, contrast capability, and spectral coverage, a two-mirror, off-axis, and unobstructed optical design, believed to be novel, has been adopted. This configuration has been simulated with a ray-tracing code, showing that theoretically more than 80% of the collimated beam energy falls within a single pixel ($20'' \times 20''$) over the whole camera field of view and that the possible contrast ratio is smaller than 1/1000. Moreover, this novel optical design is rather simple from a mechanical point of view and is compact and relatively easy to align. All these characteristics make this type of camera rather flexible and also suitable for other space missions with similar performance requirements.

OCIS codes: 110.6770, 120.4570, 220.2740, 220.4830, 350.1260, 350.6090.

1. Introduction

Rosetta is a cornerstone mission of the European Space Agency (ESA), to be launched in January 2003, dedicated to the exploration of the P/Wirtanen comet. The main mission objective is to study the nucleus of the comet and its environment in great detail for a period of nearly 2 yr.

The mission profile of the spacecraft is rather complex. In fact, the interplanetary flight allowing the approach to the comet will last 8 yr, during which one Mars and two Earth gravity assists will be done to reach the comet with a negligible velocity difference; in addition, two flybys with the Otawara and Siwa asteroids will be performed. The satellite will rendezvous with the comet in 2011 when it is still at a distance of ≈3.2 astronomical units (AU) from the Sun. At this point the relative comet–spacecraft speed value will be essentially zero, thus allowing the probe to be injected, after a sequence of highly accurate maneuvers, in an elliptical orbit with a semimajor axis between 5 and 20 comet radii around the comet itself. So, unlike the Giotto satellite, which had only a short flyby with the Halley comet in 1986, this spacecraft will follow the comet evolution along its orbit until it reaches the perihelion at ≈1 AU in 2013.

This mission profile will allow observation of many important comet activities such as sublimation of ice and outflow of gas and dust, from their very onset, when the comet is far from the Sun, to their maximum, when the comet is close to its perihelion. The primary scientific goal of this space mission is to confirm and advance theses on the cometary processes, on the origin of comets, and on their relationship with interstellar material, so as to gain insight into the origin of the solar system.[1]

The scientific payload of the satellite orbiting around the comet consists of a complementary set of both remote imaging instruments, such as imagers in the visible and the near-UV spectral ranges, spectrometers from UV to IR, radar, and *in situ* instruments, such as gas and dust mass spectrometers and a dust flux analyzer. In addition, the spacecraft will also carry a *Surface Science Package*, to be delivered

G. Naletto (naletto@dei.unipd.it), V. Da Deppo, and M. G. Pelizzo are with the Dipartimento di Elettronica e Informatica, and Centro Interdipartimentale Studi ed Attività Spaziali (Center for Studies and Activities for Space), University of Padova, Via Gradenigo, 6/A, Istituto Nazionale per la Fisica della Materia, Unity of Padova, I-35131 Padova PD, Italy. R. Ragazzoni is with the Osservatorio Astronomico di Padova, Vicolo dell'Osservatorio, 5, I-35122 Padova PD, Italy. E. Marchetti is with the European Southern Observatory, Karl-Schwarzschild-Strasse 2, D-85748 Garching bei München, Germany.

Received 7 May 2001; revised manuscript received 4 September 2001.

0003-6935/02/071446-08$15.00/0

on the surface of the nucleus to perform direct measurements of the comet soil.

The imaging system of the scientific payload plays an essential role for giving answers to some fundamental questions about the nature of cometary nuclei and about the sources of dust and gas. Since Rosetta will act in close proximity to the cometary nucleus, both narrow- and wide-field-of-view (FoV) imaging systems are necessary: The first will see in great detail portions of the surface of the comet, thus allowing the investigation of the nucleus physical properties; the latter will image large parts of the comet limb and of the inner coma, giving some important information about the outflow of dust and gas directly above the nucleus surface.[2] These two cameras, namely, the Narrow Angle Camera (NAC)[3] and the Wide Angle Camera (WAC), are the main components of the Rosetta Imaging System (OSIRIS: Optical, Spectroscopic and Infrared Remote Imaging System[4]), which will address the scientific objectives we have just described. The Center for Studies and Activities for Space (CISAS) of the University of Padova (Italy) is one of the major partners of the European consortium realizing OSIRIS, led by the Max Planck Institute für Aeronomie, and has the responsibility of realizing the WAC and the majority of the system mechanisms.

In this paper the final optical design of the WAC and its theoretical performance are presented. A brief description of the evolution of this design will also be given to show some of the modifications made to the first design during the period of defining the scientific and technical constraints. This study has led to the realization of an original all-reflecting, unobstructed, off-axis optical design, with large FoV and high contrast, satisfying all the scientific requirements of this space mission.

2. Wide Angle Camera Optical Design

The definition of the optical design of the OSIRIS/WAC has been driven by some fundamental scientific constraints. In fact, this camera is mainly designed for observing from a rather small distance the features of the weak gaseous environment surrounding the bright nucleus of the comet. This implies first of all that a rather large FoV is necessary in order to see both the edge of the nucleus and the features of emitted gas and dust. Then it is necessary to have a high contrast capability: In fact, within the camera FoV there will be both the extremely bright nucleus, which directly reflects the sunlight, and the very weak coma, where gas and dust scattered emissions have to be observed. Since the regions of greater interest for observation are those very close to the nucleus limb where there are the sources of gas and dust emission, it is important to be able to clearly separate the contribution coming from these two regions. This can be realized only if the optical contrast performance of the camera, including the residual diffraction contribution, is very high. It is also obvious that a good detector dynamics and antiblooming have to be coupled to this feature. Finally, owing to the requirement of observing the characteristic features of the comet both in the visible and in the near UV, only chromatic-insensitive optical configurations can be considered.

Table 1. Original Scientific Requirements of the WAC

Parameter	Value
Resolution at 33 km	5 m/pixel
FoV	$17.2° \times 17.2°$
Spectral range	200–1000 nm (all-reflective solution)
Detector size	2048×2048 pixels
Geometrical encircled energy	≥80% in one pixel
Stray light rejection	≥2 bounces
Contrast ratio	1/1000

All these scientific requirements strongly limit the possible optical designs, and, in particular, none of those commonly found in the literature[5–8] can be considered without significant modifications. In the following, a brief description of the historical evolution of the camera optical design is given, from the initial three-mirror configuration, to the final and simpler two-mirror one.

A. Optical Design Evolution

The scientific requirements initially considered for the camera design definition are listed in Table 1: these conditions led to an optical configuration with focal length of 80 mm, with a resolution of 150 μrad/pixel and a 25-mm-diameter entrance pupil.[9] In fact, given the initial assumptions about the comet nucleus diameter and the spacecraft orbit peri-comet, such a short focal length is necessary for seeing most of the comet when the spacecraft is very close to the nucleus; in addition, that pupil size is necessary for detecting the asteroids and the cometary nucleus when the probe is at a distance of 10^6 km. Additional constraints on the optical parameters stem from the fact that, as just described, one of the WAC's principal objectives is to detect faint structures such as gas and dust jets close to the nucleus of the comet; moreover, since the speed of the orbiter relative to the comet can be rather high at the peri-comet, this detection often has to be performed with exposure times as short as 10 ms. As a consequence, both a fast $F/3.2$ ratio is required and, to follow the weak features coming out directly above the surface, an edge transfer function dropping to 10^{-4} in the immediate neighborhood of the comet terminator is necessary.[10] This implies that obstructed solutions cannot be adopted, because the diffraction from the central obscuration increases the contrast ratio to an unacceptable level. Another limitation to the possible designs is that, because it is necessary cover a spectral range from 200 to 1000 nm, all-reflecting solutions are preferable to refractive ones: In this way no chromatic aberration is present, and possible degradation of the UV-glass performance resulting from a long stay in space is avoided.

Finally, the detector resolution element also has to

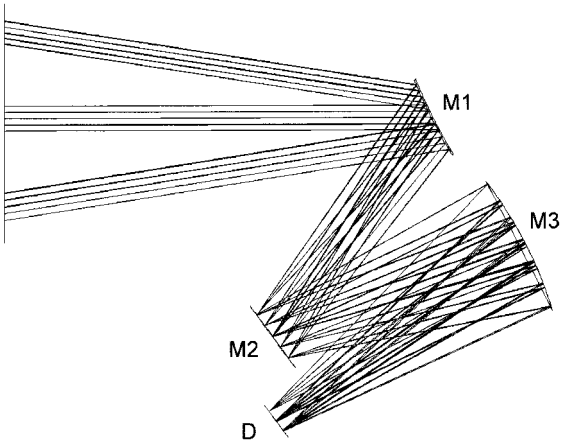

Fig. 1. WAC $F/3.2$ layout. In the drawing, M1, M2, and M3 identify the three mirrors of the camera, and D shows the detector position.

be considered in the characterization of the optical quality of the configuration. As an evaluative parameter for the soundness of the optical performance of the camera, the pixel ensquared energy (EE) can be considered: It has been decided that an EE of at least 80% in one pixel of the CCD detector is optimal.

It is also necessary to note that the optical configuration to be designed must not only satisfy all these requirements, but at the same time it has to allow a system as compact and lightweight as possible, because of the constraints of mass and size of the onboard instruments. As an obvious solution, only optical configurations with a small number of optical elements should be considered.

The simplest solution that could be used as a starting point for the optical design definition consists of an off-axis section of a two-mirror system. For example, it is well known[11] that a convex primary mirror coupled with a secondary concave one and a stop placed midway between them produces good optical performance over a rather large FoV: In fact, the convex primary mirror minimizes the aberrations depending on the FoV, whereas the secondary mirror acts essentially on the defocus term. Unfortunately, it is relatively easy to verify that in this case, owing to the very large FoV to be covered, there are some significant residual aberrations that degrade the system performance. The solution adopted to solve this problem has been to replace the stop with a folding mirror. In fact, by means of selecting a suitable shape for this mirror, the FoV-independent aberrations can be corrected, and the optical performance can be greatly enhanced. An additional advantage of this configuration is that a more compact design can be obtained, since the original two-mirror system is folded at the stop position.

Through an optimization process of this three-mirror design, the configuration shown in Fig. 1 (henceforth called WAC $F/3.2$) has been obtained, which satisfies all the mentioned scientific requirements. It consists of an off-axis section of a three-mirror coaxial system: The first mirror, M1, is a portion of a convex ellipsoid; the second one, M2, is a portion of a concave ellipsoid, rather close to a flat surface; the third mirror, M3, is a portion of a concave ellipsoid rather close to a spherical surface. The complete set of mirror parameters is summarized in Table 2. It is worth pointing out that all the mirrors are conical and that the stop, which corresponds to M2, is slightly displaced from the optical axis. Figure 2 shows the spot diagrams on the focal plane obtained by the ray-tracing simulation of this configuration. The nine spots refer to the center, edges, and corners of the whole FoV, and it is clearly seen that in all the cases the energy is rather well concentrated within a single pixel (the square boxes in Fig. 2 have 12-μm sides, which are the pixel dimensions).

Table 2. Mirror Parameters of the WAC $F/3.2$ Configuration

Mirror	Parameter
M1	Radius of curvature, −520.8 mm
	Conic constant, 2.020
M1–M2 distance	210.0 mm
M2	Radius of curvature, 1308.4 mm
	Conic constant, 172.4
M2–M3 distance	221.9 mm
M3	Radius of curvature, 342.5 mm
	Conic constant, 0.252
M3–detector distance	261.8 mm

This optical configuration was already briefly described in Ref. 10. Here we have decided to summarize its main characteristics to show that this is the only design, to our knowledge, in which an all-reflecting solution allows for coverage of such a wide FoV without introducing significant geometrical aberrations and at the same time satisfying the strong constraint about the contrast capabilities of an edge transfer function dropping at 10^{-4} within two detector pixels.

Less than 1 yr after this optical design was defined, new ground telescope observations of the comet gave a better knowledge of the cometary nucleus, and some parameters of the spacecraft orbit around the comet have to be changed. As a consequence, some of the scientific requirements also have to be redefined. So, as the mission objectives became more and more clear, some important parameters of the camera, such its FoV and focal ratio, had to be modified. In conclusion, a more modest $12° \times 12°$ FoV and a focal ratio of $F/5.6$ have been adopted.[12] Nevertheless, since two of the most important driving points, i.e., the wavelength coverage and the obtainable contrast, have been maintained almost the same, the choice of an all-reflective, unobstructed optical solution remained a mandatory requirement.

During this redefinition phase, several different optical configurations were analyzed. At the beginning the configurations were all simply small variations of the original $F/3.2$ design, because the scientific constraints were only gradually changing. But in the end, after considering relaxing some of the

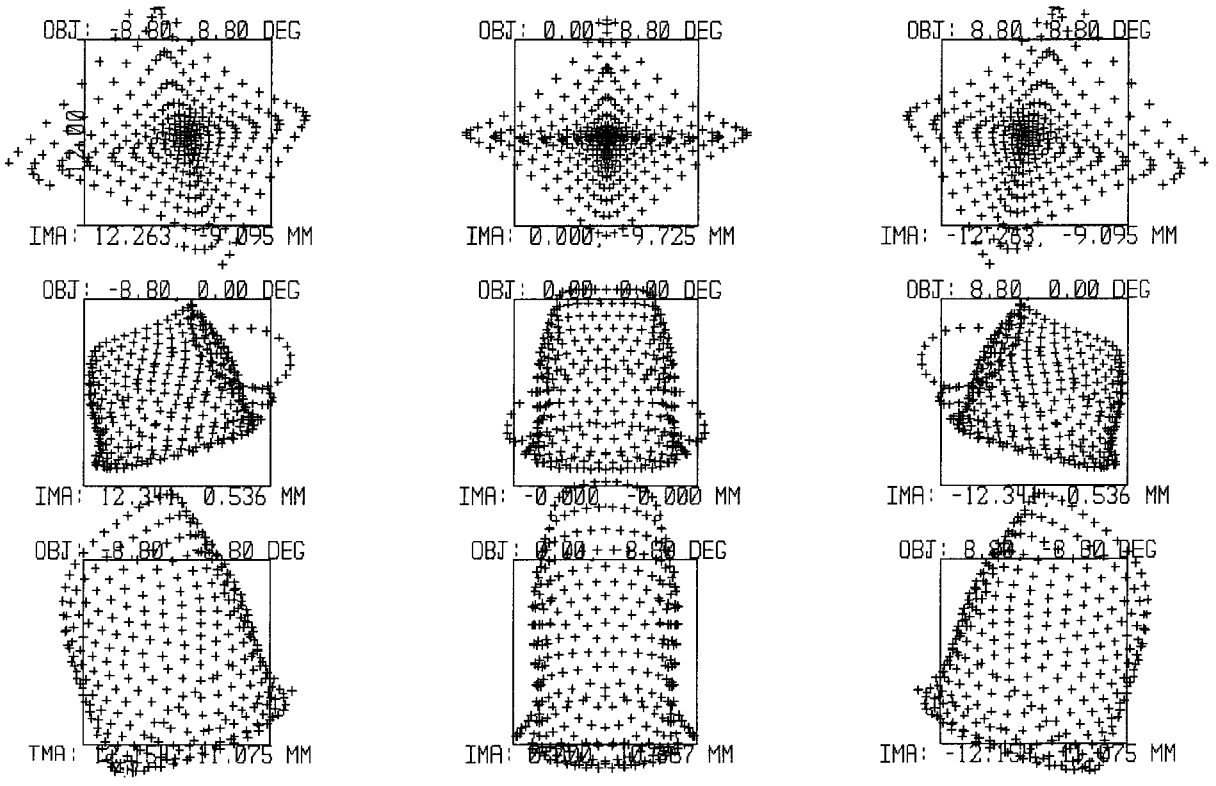

Fig. 2. WAC $F/3.2$ spot diagrams. The represented spots refer to the center, the edges, and the corners of the whole $18° \times 18°$ FoV. The boxes overlapping the spots correspond to the actual pixel size of the detector (12-μm squared in size).

parameters, it was quite natural to study the possibility of dropping one of the optical elements. This in fact could simplify the mechanical design and save in terms of both costs and alignment efforts. Finally, after analysis of a large number of optical configurations, and after a remarkable amount of optimization research, a simpler two-mirror solution has been adopted.

B. Wide Angle Camera Final Design

In this attempt of simplifying the WAC $F/3.2$ design, removing the third mirror proved to be possible. To do this, it was necessary to change the optical parameters of the other two mirrors and to move the M3 focusing capabilities to the second mirror M2. In this way, a rather unusual two-mirror optical design was obtained. It is a configuration in which the first mirror is convex, the second one is concave, and the latter also has the function of system stop.

The layout of this novel optical configuration is shown in Fig. 3, and its main characteristics are listed in Tables 3 and 4. It is a fast $F/5.6$ design combining good spatial imaging quality over a nearly $12° \times 12°$ large FoV. As shown in Fig. 3, the optical axis of the system is the geometrical axis of the primary mirror. It also corresponds to the z axis of our reference system; the y axis lies in the plane drawn in the figure, whereas the x axis is perpendicular to the others entering the drawing. The primary mirror is a convex oblate ellipsoid, and the secondary is a concave oblate ellipsoid with small conic constant; the geometrical axis of the latter is slightly tilted and shifted with respect to the optical axis. The configuration is 20° off axis and provides an unobstructed and unvignetted optical path, good baffling capabilities, flat field, provision for filter insertion, and general compactness.

As mentioned above, the aperture stop is located on the secondary mirror, and it is displaced by 5 mm from the optical axis. This location of the stop, joined to the diverging properties of the primary mirror, implies that for each direction of the incoming radiation only a small portion of the primary mirror surface is actually used (this is clear if the path of the beam rays is followed in Fig. 3); moreover, this por-

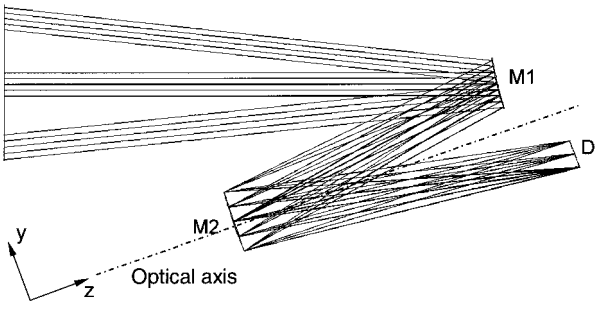

Fig. 3. WAC layout. In the drawing, M1 and M2 identify the two mirrors of the camera, and D shows the detector position. The optical axis is drawn together with the adopted orthogonal reference system.

Table 3. Main Characteristics of the WAC Final Design

Parameter	Characteristic
Optical concept	All-reflective, two-mirror, 20° off-axis design, unobstructed, unvignetted
Field of view	12°×12°
Tangential focal length	131 mm
Sagittal focal length	140 mm
Effective focal ratio	$F/5.6$
Detector size	2048×2048 pixels
Pixel size	13.5 μm×13.5 μm
Average image scale	21″ (100 μrad)/pixel
Wavelength range	240–750 nm
Refocusing	no refocusing necessary for distance range 500 m to infinity
Geometrical distortion	<2.5% along the tangential direction, <1% along the sagittal direction

tion is obviously different for each direction. This is essentially how this configuration permits small aberrations over such a wide FoV. In fact, since light beams coming from different directions impinge on different portions of the primary mirror, the surface of this mirror can be shaped *differently* on each of these portions, in an optimal way for correcting the field aberrations associated with that direction. Obviously, this optimization process of the M1 surface cannot be done perfectly, but, thanks to the relatively small input pupil required, in this case the results are highly satisfactory.

The actual design also includes a set of 14 filters, distributed on two independent wheels, with both narrow and wide bands for observations of specific lines and of continuum diffused by the comet. These optical elements are inserted after M2, so they work in converging light. Because of the $F/5.6$ aperture of the system, this gives a lower limit of ~4 nm to the possible filter narrow bandwidth. These filters work both in the visible and in the near UV, and the materials used are obviously different: OG550, OG515, and KG3 for the visible ones and Suprasil for the others. Their index of refraction varies with the wavelength, and, since there is no mechanism that allows the adjustment of the focus position, different filter thicknesses have been adopted. For evaluating the filter thicknesses, the following equation has been used:

$$t = \frac{\Delta z_o}{1 - (1/n)}, \tag{1}$$

where t is the filter thickness and n is average refraction index of the glass in the considered bandwidth. Δz_o is the variation of the focus position along the optical axis introduced by a reference filter, with respect to the focus position without any filter; this variation, whose value is 1.6 mm, has to be the same for all the filters in order to keep the detector in a fixed place. The various filter thicknesses obtained in this way vary between 4.57 and 4.94 mm, depending on the glass and on the bandwidth.

Table 4. Main Optical Parameters of the WAC Final Design[a]

Parameter	Value
Central ray direction	−20° off axis about x
M1	Radius of curvature, −406.6 mm Conic constant, 5.708
M1–M2 distance	287.1 mm
M2	Radius of curvature, 400.0 mm Conic constant, 0.166 y decenter, +5 mm tilt about x, +0.725°
M2–detector distance	337.5 mm

[a]The adopted reference system is the one described in the text, and shown in Fig. 3.

3. Optical Performance of the Wide Angle Camera Two-Mirror Design

To evaluate the image quality of the system, the two-mirror camera design that we have just described was simulated with a ray-tracing code. By means of this code it was possible to optimize the optical parameters of the configuration so as to minimize the spot diagram sizes on the focal plane, to obtain a point-spread function (PSF) satisfying the contrast requirement (see Fig. 6), and to maximize the EE in a single pixel. Obviously, this optimization process has been realized for all the different beam directions in the FoV.

Figure 4 shows the spot diagrams at the center, at the edges, and at the corners of the FOV; the square boxes correspond to the pixel size (13.5-μm side). It is clear from this figure that the geometrical performance of the camera is optimal, with residual aberrations essentially lower than the pixel size. We have to point out that this is the result of a pure geometrical ray tracing, which does not consider any diffraction effect. In any case, it is possible with the simulation code to have an estimate of the diffraction contribution to the spots. The global effect is summarized in Fig. 5, where the EE scaled by diffraction at $\lambda = 387.5$ nm is given as a function of the half-width from the centroid (the wavelength for the evaluation of the diffraction has been selected at $\lambda = 387.5$ nm because half the WAC filters have bands below this value and the other half above). It is clear from this figure that the residual diffraction is negligible, leaving an EE within a single pixel of the order of 90%.

In Fig. 6 the contrast capability of the camera is shown: the two plots represent the profile of the camera PSF evaluated at $\lambda = 387.5$ nm along two perpendicular planes (tangential and sagittal) passing through the PSF peak. It is evident that the spot intensity at a 2-pixel distance from the peak is of the order of 1/10000 of the peak intensity, essentially satisfying the contrast requirement. A very small asymmetry in the tangential PSF, owing to the off-axis nature of this camera, is also noticeable.

Because of the off-axis design, the optical elements have different powers in the sagittal and in the tangential planes, so there are two different focal lengths

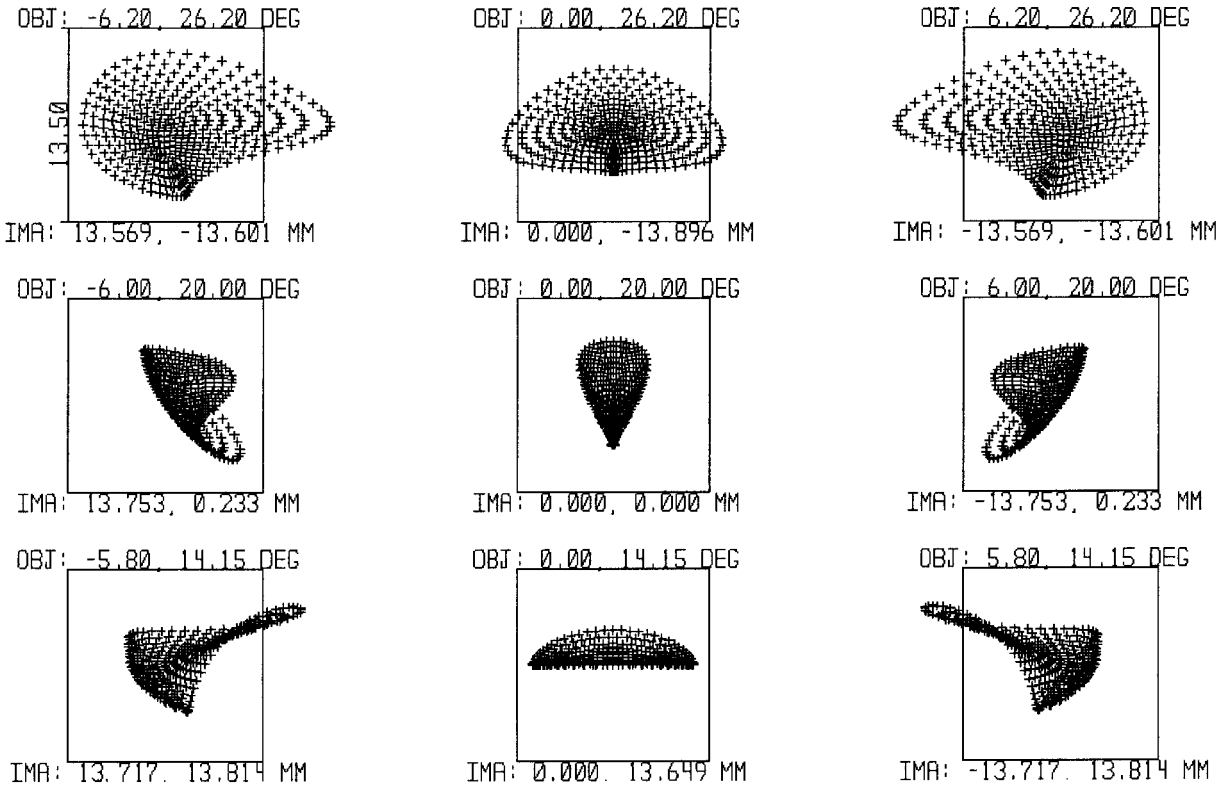

Fig. 4. WAC spot diagrams. The represented spots refer to the center, the edges, and the corners of the whole 12° × 12° FoV. The boxes overlapping the spots correspond to the actual pixel size of the detector (13.5 μm squared size).

in these two planes. This implies that ~6% anamorphic distortion is present, with a sagittal plane focal length f_s = 140 mm and a tangential plane focal length f_t = 132 mm. Because of this difference, to a first approximation a circular object will be reimaged into an ellipse with its axes proportional to the tangential and the sagittal focal lengths. Figure 7 shows how this distortion works over the system's whole FoV.

In the analysis of this optical design, obviously the study of the alignment tolerances has also been performed, and we describe the obtained results. This will provide an idea about the amount of work necessary to align the system and at the same time about the sensitivity of the stiffness of the optical bench over which the optics have to be mounted. The criteria assumed in this analysis are that the image should not degrade by more than 30% as FWHM of the nominal spot size and that it should not be dis-

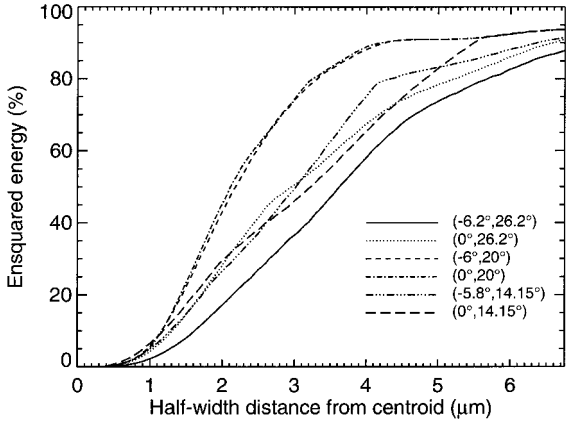

Fig. 5. Plot of the percentage of the collimated beam energy falling in a squared box of specified half-size. This plot shows that the percentage of energy falling in a single pixel of the detector (6.75-μm half-size) is always of the order of 90%.

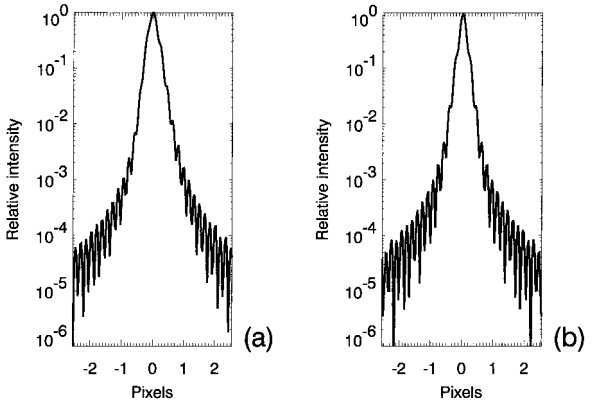

Fig. 6. Plots of the camera PSF profiles evaluated at λ = 387.5 nm along two perpendicular directions: (a) in the tangential plane, (b) in the sagittal one.

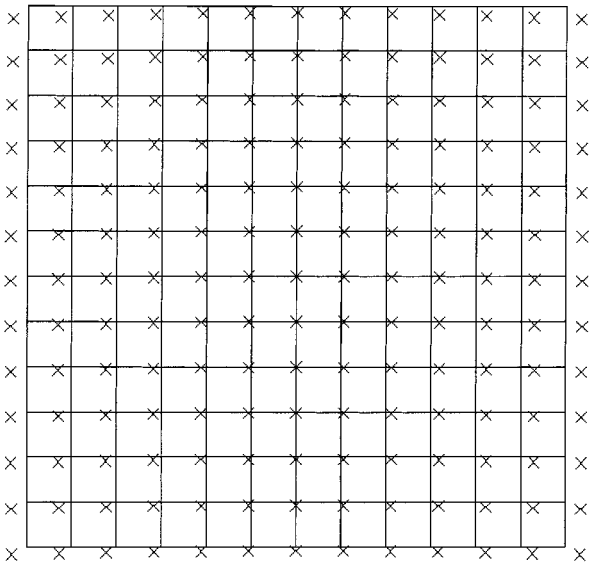

Fig. 7. Anamorphic magnification of the WAC: In this drawing, the grid corresponds to the ideal nondistorted image; the crosses, to the actual position of the grid vertex as imaged by the camera.

placed by more than 1/3 of a pixel during a typical exposure time.

In this study we have considered two different types of tolerance: one relative only to the alignment phase and the other relative to the on-flight stability. In the first case, for each optical element, the maximum displacement or rotation for which the consequent image degradation can be recovered by suitable movements of the other optical elements of the system is evaluated. The results of the tolerance analysis are summarized in Table 5. It is evident that the alignment of this camera is not a critical issue, because the system is rather tolerant to shifting and tilting of the elements. Even if the mirrors are not in their correct position, it is still possible to optimize the optical performance of the camera. Because of these relaxed alignment tolerances, we have adopted the philosophy of keeping M1 fixed and adjusting only the positions of M2 and of the detector. Here fixed means that M1 can simply be mechanically positioned at its nominal place inside the camera structure, the mechanical tolerances being smaller than the optical ones.

Table 5. Alignment and In-Flight Tolerances of the WAC

	Δx, Δy (mm)	Δz (mm)	$\Delta\Phi_x$, $\Delta\Phi_y$ (deg)	$\Delta\Phi_z$ (deg)
Alignment tolerances				
M1	±1	±2	±0.5	±0.3
M2	±1	±2	±0.3	—
D	±1	±2	±0.3	—
In-flight long-term tolerances				
M1	±0.1	±0.01	±0.1	±0.2
M2	±0.1	±0.01	±0.015	—
D	±0.1	±0.01	±0.05	—

More critical are the tolerances for maintaining the system in-flight optical performance. In this case we have considered two different subsets of tolerances: the short-term ones, which have to be satisfied during a single exposure, and the long-term ones, which have to be maintained during the whole mission. The former are relative to simple displacement of the image with respect to the detector position, whereas the latter imply a degradation of the optical quality. Actually, since the maximum exposure times will be of the order of a few seconds, the short-term tolerances are not critical and are not here listed. More stringent, rather, are the long-term ones (see Table 5). For example, a relative misplacement of M1 and M2 of the order of only 10 μm along the optical axis gives a degradation of ~30% of the FWHM for the spot at the center of the FoV. This fact has implied rather stringent tolerances on the mechanical design of the camera that have to be satisfied to keep the system aligned throughout its mission lifetime.

4. Conclusions

In this paper the characteristics and the foreseen performance of the OSIRIS Wide Angle Camera (WAC) design have been presented. This design, believed to be novel, which is off-axis, all-reflecting, unobstructed, and has only two conical optical elements, allows coverage of a 12° × 12° FoV with a spatial resolution of 20″/pixel and high contrast. Nominally, at least 90% of the beam energy coming from one direction falls in a single pixel, and a contrast as high as 10^{-4} is obtained at a two-pixel distance. This type of performance allows the camera to satisfy all the scientific requirements, which is essentially the capability of simultaneously detecting a large portion of the bright edge of the comet nucleus together with the weak features of the coma, where light is scattered by gas and dust.

The camera performance described in this paper is only theoretical, as obtained by means of a ray-tracing simulation. Currently, some activity is in progress in our laboratories to validate these results. Several efforts have been dedicated to realizing the optics: In particular, the first mirror, which is the most difficult to fabricate, has been checked with an *ad hoc* quasi null-lens system. The mirrors obtained in this way are within the specifications given to the manufacturer, which makes us confident that we will be able to obtain performance close to that expected of the assembled system. Describing the actual performance obtained by the system will be the subject of a future paper.

The authors thank F. Angrilli, C. Barbieri, and G. Tondello, who are the Italian investigators of this project, and H. U. Keller, who is the principal investigator of OSIRIS. Thanks are also extended to the whole WAC team, who contributed in different ways to the design of this instrument. Finally, we acknowledge the Italian Space Agency, who financed this project.

References and Note

1. A. Bar-Num, A. Barucci, E. Bussoletti, A. Coradini, M. Coradini, J. Klinger, Y. Longherin, R. J. Laurence, J. A. M. Mc Donnel, A. Milani, B. Picardi, C. Pillinger, G. Schwen, D. Stoffer, and H. Wänke, "Rosetta Comet Rendezvous Mission, study report of ESA," ESA Publication SCI(93) (European Space Agency, Paris, 1993), Vol. 7.
2. N. Thomas, H. U. Keller, E. Arijs, C. Barbieri, M. Grande, P. Lamy, H. Rickman, R. Rodrigo, K.-P. Wenzel, M. F. A'Hearn, F. Angrilli, M. Bailey, M. A. Barucci, J.-L. Bertaux, K. Briess, J. A. Burns, G. Cremonese, W. Curdt, H. Deceuninck, R. Emery, M. Festou, M. Fulle, W.-H. Ip, L. Jorda, A. Korth, D. Koschny, J.-R. Kramm, E. Kürt, M. L. Lara, A. Llebaria, J. J. Lopez-Moreno, F. Marzari, D. Moreau, C. Muller, C. Murray, G. Naletto, D. Nevejans, R. Ragazzoni, L. Sabau, A. Sanz, J.-P. Sivan, and G. Tondello, "OSIRIS—the optical, spectroscopic and infrared remote imaging system for the Rosetta orbiter," Adv. Space Res. **21,** 1505–1515 (1998).
3. K. Dohlen, M. Saisse, G. Claeysen, and J.-L. Boit, "Optical designs for the Rosetta narrow-angle camera," Opt. Eng. **35,** 1150–1157 (1996).
4. The name OSIRIS has been maintained since the time when spectroscopic and infrared imaging capabilities of the instrument were also foreseen.
5. D. J. Schroeder, "All-reflecting Baker–Schmidt flat field telescopes," Appl. Opt. **17,** 141–144 (1978).
6. R. B. Johnson, "Wide field of view three-mirror telescopes having a common optical axis," Opt. Eng. **27,** 1046–1050 (1988).
7. A. G. Dall'Era, "Wide angle, reflective optical systems for infrared applications," in *Lens and Optical System Design*, H. Zuegge, ed., Proc. SPIE **1780,** 817–824 (1992).
8. D. G. Torr, M. R. Torr, M. Zukic, J. F. Spann, and R. B. Johnson, "Ultraviolet imager for the International Solar Terrestrial Physics Mission," Opt. Eng. **32,** 3060–3068 (1993).
9. R. Ragazzoni, G. Naletto, M. Turatto, and E. Marchetti, "Preliminary optical design for Plures and Rosetta," in *Ultraviolet Technology V*, R. E. Huffman and C. G. Stergis, eds., Proc. SPIE **2282,** 162–168 (1994).
10. R. Ragazzoni, G. Naletto, C. Barbieri, and G. Tondello, "An optical design for the Rosetta Wide Angle Camera," in *Space Telescopes and Instruments*, P. Y. Bely and J. B. Breckinridge, eds., Proc. SPIE **2478,** 257–268 (1995).
11. J. M. Sasian, "Design of a Schwarzschild flat field, anastigmatic, unobstructed, wide-field telescope," Opt. Eng. **29,** 1–5 (1990).
12. G. Naletto, E. Marchetti, R. Ragazzoni, "Two-mirror planetary camera with an off-Rowland UV spectrograph for the Rosetta mission," in *Space Telescopes and Instruments II*, P. Y. Bely and J. B. Breckinridge, eds., Proc. SPIE **2807,** 238–247 (1996).